TMT-AGE: numerical simulation of a new tomographic reconstruction method for wide FoR MOAO

Yoshito H. Ono[a,b], Akiyama Masayuki[a], Shin Oya[b]

[a]Astronomical Institute, Tohoku University, 6-3 Aoba, Aramaki, Aoba-ku, Sendai, Miyagi 980-8578, Japan;
[b]Subaru Telescope, NAOJ, 650 North A ' ohoku Place, Hilo, Hawaii 96720, USA

ABSTRACT

We are conducting a concept study on a wide field of regard (FoR) Multi-Object Adaptive Optics (MOAO) system for Thirty Meter Telescope (TMT-AGE: TMT-Analyzer for Galaxies in the Early universe). The main science target of TMT-AGE is high-redshift galaxies. Considering the small number density of high-redshift galaxies, enlarging the FoR of an MOAO system up to around $10'$ is critical. In order to increase the FoR of an MOAO system, we propose a new tomographic reconstruction method. In the new method, we use atmospheric wind profiles and WFS measurements at previous time steps to increase the number of virtual measurement points of atmospheric turbulence layers for tomographic reconstruction. We present the results of numerical simulations with the new tomography method. The simulations show the new method can reduce the tomographic error in a wide FoR.

Keywords: TMT, Multi-Object Adaptive Optics, tomography

1. INTRODUCTION

Multi-Object Adaptive Optics (MOAO) is an approach of wide-field Adaptive Optics (AO). MOAO applies AO corrections for multiple objects in a field of regard (FoR) and realize high spatial resolution observations of the multiple objects. For Thirty Meter Telescope (TMT), an instrument incorporating MOAO and multiple integral field units is proposed to reveal properties of high-redshift galaxies, called near-InfraRed Multi-Object Spectrograph (IRMOS) [1]. One of key parameters of an MOAO system is the size of a FoR. Since very high-redshift galaxies at redshift larger than 5 have small number density, wide FoR of around $10'$ diameter is necessary to utilize the high multiplicity of an MOAO system for such targets. However, the MOAO system of IRMOS is considered capability over a $5'$ FoR. Therefore, we are conducting a concept study on a wide-field MOAO system for TMT, which has a wide FoR of around $10'$ diameter (TMT-AGE: TMT-Analyzer for Galaxies in the Early universe, [2]).

The key technique for enlarging the FoR of an MOAO system is a tomographic reconstruction which estimates the 3-dimensional atmospheric wavefront disturbance using information from multiple guide stars (GS). The size of a FoR and the accuracy of a tomographic reconstruction of an MOAO system depend strongly on a configuration of multiple GSs. Wider GS separation can realize wider FoR, but cause large tomographic error because the area of the gap regions of the high-altitude atmospheric turbulence that is covered only by one or no GS meta-pupil increases with the separation (Figure 1). In the case of laser guide stars (LGS), the influence is worse due to the cone effect. Therefore increasing the FoR of an MOAO system with keeping the tomographic reconstruction accuracy is difficult. In this paper, we present a new tomographic reconstruction method to increase the FoR of an MOAO systems.

The new method uses atmospheric wind profiles and WFS measurements at previous time steps to increase the number of measurement points of atmospheric turbulence layers for tomographic reconstruction. Thanks to the displacement of the previous measurements due to winds, we can fill in the gap regions with previous measurements and expanding the FoR of an MOAO system without increasing the tomographic error. We

Further author information: (Send correspondence to Yshito H. Ono)
Yoshito H. Ono: E-mail: ono@naoj.org, Telephone:+1-808-934-5910

also present a method to estimate wind speed and direction at each altitude, which is necessary for the new tomographic reconstruction method. Through numerical simulations of an MOAO system for 30m aperture telescope at Mauna Kea, we demonstrate that the new method reduces a tomographic error compared to a classical tomographic method at the same configuration of LGS.

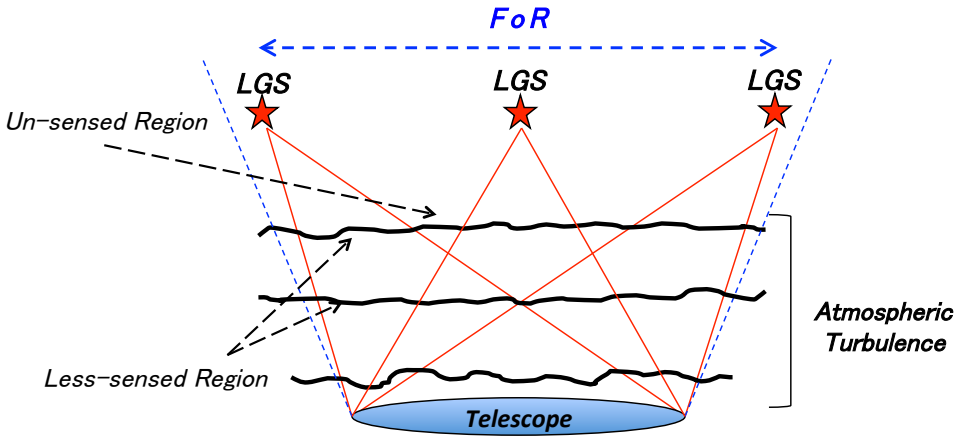

Figure 1. Schematic geometry of atmospheric turbulence layers and LGS meta-pupils. There are the gap regions in the high-altitude atmospheric turbulence that is covered only by one or no GS meta-pupil.

2. METHOD

In this section, we explain a classical tomographic method at first. Then, we present the new tomographic method and the method to estimate wind speed and direction at each altitude.

2.1 Measurement Model

Using Shack-Hartmann Wave-Front Sensor (WFS), the linear equation between the incoming wavefront $\boldsymbol{w_j}$ from jth LGS of $N_{\rm lgs}$ and the gradients measured by jth WFS observing the jth LGS at time t is given by

$$\boldsymbol{s_j}(t) = \boldsymbol{G_j}\boldsymbol{w_j}(t) + \boldsymbol{\eta_j}(t), \tag{1}$$

where $\boldsymbol{G_j}$ is a gradient operator of Fried geometry for jth WFS, and $\boldsymbol{\eta_j}(t)$ is a measurement noise vector. Assuming that the turbulent atmosphere consists of thin layers in total $N_{\rm layer}$ located in different altitudes h_l, the phase $\boldsymbol{w_j}$ of light from jth LGS at time t is distorted as

$$\boldsymbol{w_j}(t) = \sum_{l=1}^{N_{\rm layer}} \boldsymbol{P_{l,j}}\boldsymbol{\phi_l}(t) = \boldsymbol{P_j}\boldsymbol{\phi}(t). \tag{2}$$

Here, $\boldsymbol{P_{l,j}}$ is a projection matrix which extracts the wavefront within the jth LGS meta-pupil from the lth atmospheric turbulence $\boldsymbol{\phi_l}$ at altitude h_l with a bilinear interpolation; $\boldsymbol{\phi}$ and $\boldsymbol{P_j}$ are a vector and matrix concatenating the atmospheric turbulences of $N_{\rm layer}$ and projection matrices, respectively. Combining Eq.(1) and Eq.(2) and considering the all LGSs, the equation connecting the measurements of the all WFSs at time t through the all atmospheric turbulences at time t can be represented as follows:

$$\boldsymbol{s}(t) = \boldsymbol{G}\boldsymbol{P}\boldsymbol{\phi}(t) + \boldsymbol{\eta}(t). \tag{3}$$

where $\boldsymbol{s}$ and $\boldsymbol{\eta}$ are expansion vector of $\boldsymbol{s_j}$ and $\boldsymbol{\eta_j}$ respectively, and $\boldsymbol{G}$ is a block diagonal matrix, which is $\boldsymbol{G} = \mathrm{diag}(\boldsymbol{G_j}, \cdots, \boldsymbol{G_{N_{\rm lgs}}})$.

2.2 Tomographic Reconstruction

We use Minimum Variance Reconstructor[3] (MVR) to estimate the atmospheric turburences. The MVR provides an optimal solution for Eq.(3) using the statistics of the atmospheric turbulence and the WFS measurement noise. We can estimate $\boldsymbol{\phi}$ by minimizing

$$E(||\boldsymbol{\phi} - \hat{\boldsymbol{\phi}}||^2). \tag{4}$$

The hat symbol indicates estimated quantities. The solution to this problem is given by

$$(\boldsymbol{P}^T\boldsymbol{G}^T\boldsymbol{G}\boldsymbol{P} + \sigma^2\boldsymbol{L}^T\boldsymbol{L})\hat{\boldsymbol{\phi}}(t) = \boldsymbol{P}^T\boldsymbol{G}^T\boldsymbol{s}(t), \tag{5}$$

where $\boldsymbol{L}$ is proportional to a discretization of the Laplacian operator and σ^2 is the variance of WFSs measurements. Eq.(5) is of the form $\boldsymbol{A}\hat{\boldsymbol{x}} = \boldsymbol{b}$ and the all matrices included in Eq.(5) are sparse. Such problems can be solved efficiently by using iterative methods[4][5]. In this paper, we use a Conjugate Gradient (CG). In the following, we call Eq.(5) a classical method.

After the tomographic reconstruction, the command (or the shape) of each Deformable Mirror (DM) in direction of a science target is calculated with the estimated atmospheric turbulences. In this simulation, the DM wavefronts $\hat{\boldsymbol{w}}_{\boldsymbol{dm}}$ are estimated with a bilinear interpolation.

$$\hat{\boldsymbol{w}}_{\boldsymbol{dm,k}} = \boldsymbol{P}_{\boldsymbol{k}}\hat{\boldsymbol{\phi}}(t) \quad (k = 1, \cdots, N_{\text{target}}) \tag{6}$$

2.3 New Tomographic Reconstruction

Under the assumption of Taylor's frozen-flow hypothesis, evolution of atmospheric turbulences can be described as the shift of each layer due to the wind $\boldsymbol{v} = (v_x, v_y)$ at each altitude. Introducing a projection matrix $\boldsymbol{P}_{\boldsymbol{l,j}}(\Delta t)$ which takes account of the displacements of jth LGS meta-pupil at altitude h_l due to a wind $\boldsymbol{v}_{\boldsymbol{l}}$ within a time interval Δt, the relation between measured gradients of the all WFSs at time $(t - \Delta t)$ and the all atmospheric turbulences at time t is given by

$$\boldsymbol{s}(t - \Delta t) = \boldsymbol{G}\boldsymbol{P}(\Delta t)\boldsymbol{\phi}(t) + \boldsymbol{\eta}(t - \Delta t). \tag{7}$$

Concatenating Eq.(7) with Eq.(3) and using MVR, we can estimate the atmospheric turbulence with measurements taken both current and previous time step as follows.

$$(\boldsymbol{P'}^T\boldsymbol{G'}^T\boldsymbol{G'}\boldsymbol{P'} + \sigma^2\boldsymbol{L}^T\boldsymbol{L})\hat{\boldsymbol{\phi}}(t) = \boldsymbol{P'}^T\boldsymbol{G'}^T\boldsymbol{s'}, \tag{8}$$

where $\boldsymbol{s'} = [\boldsymbol{s}^T(t) \;\; \boldsymbol{s}^T(t - \Delta t)]^T$, $\boldsymbol{G'} = \text{diag}(\boldsymbol{G}, \boldsymbol{G})$, and $\boldsymbol{P'} = [\boldsymbol{P}^T \;\; \boldsymbol{P}^T(\Delta t)]$. The DM wavefronts is estimated with Eq.(6). Wind speeds and directions at each altitude are necessary in order to make $\boldsymbol{P'}(\Delta t)$. Next, we present how to estimate wind information.

2.4 Estimation of Wind Speeds and Directions

To date, two methods for estimate wind speeds and directions of multiple atmospheric layers. One is using spatio-temporal cross correlation of measured WFS data[6], which was developed from the SLODAR method[7]. In the SLODAR method, the peaks of spatial cross correlation for two WFSs data with no-time delay give the information of turbulence altitudes. Performing spatio-temporal cross correlation with time-delayed WFSs data, each correlation peak on the correlation map moves according to the wind speed and direction. We can estimate the wind speeds and directions by tracking this movement of each peak. However, it is difficult to detect and track multiple peaks on a correlation map. The other way is using fourier technique, called Fourier Wind Identification (WFI)[8], but this method doesn't evaluate turbulence altitudes.

In this paper, we propose a method to estimate wind speed and wind direction at each altitude using the turbulent atmosphere estimated by a tomographic reconstruction. Tomographic reconstruction provides the phase map at each altitude. Using a projection matrix $\boldsymbol{P}_{\boldsymbol{l,j}}$ and a gradient operator $\boldsymbol{G}_{\boldsymbol{j}}$, the estimated slope map at each altitude in each LGS direction can be calculated.

$$\hat{\boldsymbol{s}}_{\boldsymbol{l,j}}(t) = \boldsymbol{G}\boldsymbol{P}_{\boldsymbol{l,j}}\hat{\boldsymbol{\phi}}(t), \tag{9}$$

$\hat{\boldsymbol{s}}_{\boldsymbol{l,j}}(t)$ is the estimated slope at altitude of lth atmospheric screen in direction of jth LGS. Performing temporal correlation to the estimated slopes $\hat{\boldsymbol{s}}_{\boldsymbol{l,j}}$ and tracking the peaks give the wind direction and speed at altitude of h_l. Since $\hat{\boldsymbol{s}}_{\boldsymbol{l,j}}$ includes only one atmospheric layer component, there is only one peak expected on the correlation map ideally and tracking the peak is easier than the above like method.

3. SIMULATION

The setup of our numerical simulations is as follows. The diameter of the circular aperture is set to 30m. An atmospheric model of seven layers with $r_0 = 0.156$m and $L_0 = 30$m is adopted, which is typical condition at the summit of MaunaKea and used in [9]. The altitudes, C_N^2 fraction, and wind speeds are listed in Table 1. Each atmospheric layer is assumed 100% frozen flow layer. The wind directions are random and the wind speeds do not change with time. Shack-Hartmann WFSs are used with 0.5m subaperture and RMS read error of $\sigma_e = 5$ electrons. The brightness of LGSs corresponds to 700 electrons per subaperture. Tomographic reconstruction is performed with two configurations of eight LGSs shown in Figure 2: one configuration is the nominal TMT-IRMOS design(Open green star), the other is wider configuration(Filled red star).

Although the altitudes and C_N^2 values of atmospheric layers must be measured on-sky during observation, for example with SLODAR, we assume the information is known perfectly in this simulation. The time-delay due to calculation time and WFS exposure are not considered.

Altitude [km]	0	0.5	1	2	4	8	16
C_N^2 fraction	0.5960	0.0963	0.0325	0.0372	0.0869	0.0684	0.0826
Wind speed [m/s]	7.817	8.690	9.738	12.357	18.953	24.215	5.783

Table 1. Altitude, C_N^2 fraction, and wind speeds of atmospheric layers.

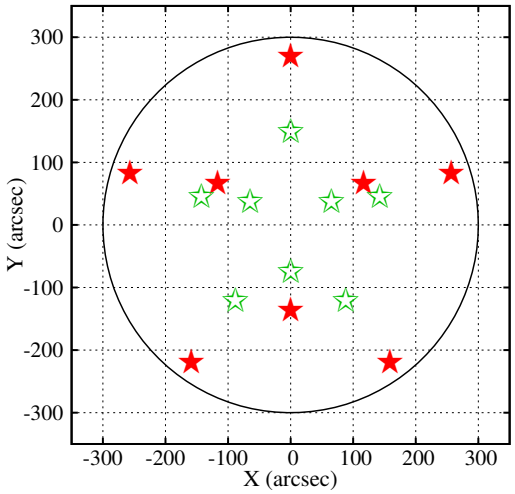

Figure 2. LGS configuration. Open green star: nominal TMT-IRMO configuration which is optimize for a 5′ FoR. Filled red star: wider configuration.

4. RESULTS

4.1 Estimation of Wind Speeds and Directions

Wind estimation is performed using 10s simulated WFSs data. The estimation error of wind speeds are less than 1 [m/s] for all the layers, except 2.3 [m/s] at 8km. It is due to the highest wind speeds of 24[m/s] at the layer in this simulation. The errors of wind directions are very small for all altitude, which are less than 1 degree.

Note that this is a result with 100% frozen flow assumption and perfect information of atmospheric layer altitudes. Indeed, the time scale of frozen flow is limited and the correlation peak becomes fainter with time [6]. This affects the accuracy of the detection of the correlation peaks. Also, if a tomographic reconstruction for a layer is performed at middle of two real atmospheric layers, the estimate can mix the two atmospheric layers. In this case, two peaks corresponding to the atmospheric layers may appear on a correlation map and

identifying multiple peak can be difficult. We will evaluate the accuracy of the wind estimation method with the uncertainties of the altitudes of atmospheric layers in a future work.

4.2 Tomographic Reconstruction

The simulation results are presented in Figure 3. We perform the classical tomography method for the two configurations of LGSs and the new tomography method for only the wider configurations. For the new method, the measurements at 0.1s previous time step are used, $\Delta t = 0.1s$, and the estimated wind speeds and directions are also used. The accuracy of tomographic reconstructions is evaluated with residual wavefront error(WFE). Using the classical method for the nominal TMT-IRMOS configuration(open green circle in Figure 3), the WFE within the central $5'$ is less than 200nm but the WFE of the outside of the central $5'$ FoR increases steeply with radius much higher than 300nm, because there is no LGS at the outer region of the central $5'$. In the case of the wide configuration(filled red circle in Figure 3), the WFE of the outer region of FoR is smaller than that of the TMT-IRMOS configuration but the central WFE increases up to 250nm due to more gap regions which are less covered with LGSs meta-pupils.

With the new tomographic reconstruction method for the wider configuration (filled red square in Figure 3), the WFE within the central $5'$ FoR reduces to less than 200nm and the WFE in $8'$ FoR is less than 250nm. It is because the wider configuration has the gap regions which are un-sensed or less-sensed with LGS meta-pupils and the new method can fill the gap regions with measurements at previous time step. In this simulation, the estimation errors of both speeds and directions do not affect on the results of tomography. The displacement error within 0.1s due to wind estimation error is less than 25cm. Since this is half of DM segment size, a tomographic error due to the error of wind estimation is smaller than the fitting error. These results show the new tomographic reconstruction can increase the accuracy of reconstruction within the FoR and is beneficial to expand the FoR of MOAO.

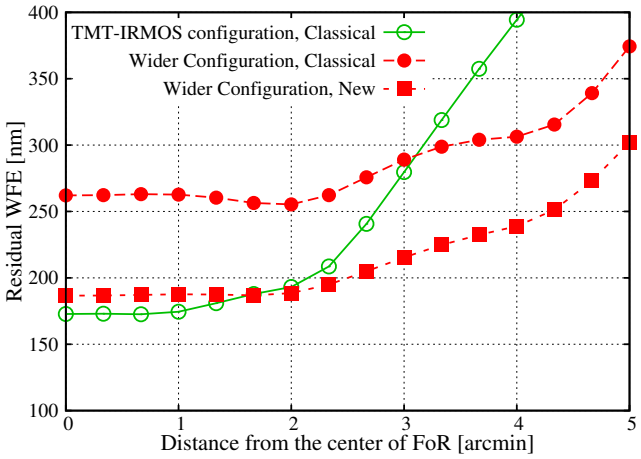

Figure 3. The residual WFE as a function of field radius. Open green and filled red symbol indicate results with the TMT-IRMOS configuration and the wider configuration, respectively. The circle and square show the results with classical and new tomographic reconstruction method, respectively.

5. CONCLUSIONS AND FUTURE WORK

We propose a new tomographic reconstruction method using measurements at previous time steps and wind information to increase the FoR of MOAO systems and evaluate the method with numerical simulations. We also introduce a method to estimate wind speeds and directions at each altitude. The wind profiles can be estimated with sufficient accuracy under assumption of 100% frozen flow and perfect knowledge of altitudes of atmospheric turbulences. With estimate of wind speeds and directions, the new tomographic reconstruction method reduces WFE to less than 250nm for the wider LGS configuration in $8'$ FoR.

A future work is to perform a SLODAR simulation to evaluate the estimation accuracy of atmospheric turbulence altitudes. Then, we will be able to evaluate the wind estimation method in a more realistic situation. Further, we will try these new methods with on-sky WFS data which were taken by Subaru Telescope with RAVEN[10], which is an MOAO technology and science demonstrator developed by University of Victoria and HIA.

ACKNOWLEDGMENTS

This work is supported by NAOJ Japanese TMT office strategic research and development funding of FY2012, FY2013, and FY2014. M.A. is supported by JSPS KAKENHI Grant-in-Aid for Young Scientists (B) 23740140 and Grant-in-Aid for Scientific Research (B) 26287027.

REFERENCES

[1] Eikenberry, S., Andersen, D., Guzman, R., Bally, J., Cuevas, S., and et al, "IRMOS: The near-infrared multi-object spectrograph for the TMT," *Proc. SPIE* **6269**, Ground–based and Airborne Instrumentation for Astronomy, 62695W (2006).

[2] Akiyama, M., Ono, Y., Oya, S., and et al, "TMT-AGE: wide field of regard multi-object adaptive optics for TMT," *Proc. SPIE* **this volume**, Adaptive Optics Systems IV (2014).

[3] Ellerbroek, B. L., "Efficient computation of minimum-variance wave-front reconstructors with sparse matrix techniques," *J. Opt. Soc. Am. A* **19**, 1803–1816 (2002).

[4] Gilles, L., Vogel, C. R., and Ellerbroek, B. L., "Multigrid preconditioned conjugate-gradient method for large-scale wave-front reconstruction," *J. Opt. Soc. Am. A* **19**, 1817–1822 (2002).

[5] Vogel, C. R. and Yang, Q., "Multigrid algorithm for least-squares wavefront reconstruction," *Appl. Opt* **45**, 705–715 (2006).

[6] Corts, A., Rudy, A., Neichel, B., Poyneer, L., Ammons, S., and Guesalaga, A., "Analysis of the frozen flow assumption using gems telemetry data," in [*Proceedings of the Third AO4ELT Conference*], Esposito, S. and Fini, L., eds., INAF - Osservatorio Astrofisico di Arcetri, Firenze (2013).

[7] Wilson, R. W., "Slodar: measuring optical turbulence altitude with a shack—hartmann wavefront sensor," *Monthly Notices of the Royal Astronomical Society* **33**, 103–108 (2002).

[8] Poyneer, L., van Dam, M., and Vran, J.-P., "Experimental verification of the frozen flow atmospheric turbulence assumption with use of astronomical adaptive optics telemetry," *J. Opt. Soc. Am. A* **26**, 833–846 (2009).

[9] Andersen, D. R., Jackson, K. J., Blain, C., Bradley, C., Correia, C., Ito, M., Lardire, O., and Vran, J.-P., "Performance modeling for the raven multi-object adaptive optics demonstrator," *Publications of the Astronomical Society of the Pacific* **124**, 469–484 (2012).

[10] Andersen, D. R., Bradley, C., Lardire, O., Blain, C., Correia, C., and et al, "Status of the raven moao science demonstrator," *Proc. SPIE* **8447**, Adaptive Optics Systems III, 84473F (2012).